

Towards a Pixel TPC: construction and test of a 32 chip GridPix detector

M. van Beuzekom^a, Y. Bilevych^b, K. Desch^b, S. van Doesburg^a,
H. van der Graaf^a, J. Kaminski^b, P.M. Kluit^a, N. van der Kolk^a, C.
Ligtenberg^a, G. Raven^a, J. Timmermans^a

^a*Nikhef, Science Park 105, 1098 XG Amsterdam, The Netherlands*

^b*Physikalisches Institut, University of Bonn, Nussallee 12, 53115 Bonn,
Germany*

Abstract

A Time Projection Chamber (TPC) module with 32 GridPix chips was constructed and the performance was measured using data taken in a test beam at DESY in 2021. The GridPix chips each consist of a Timepix3 chip with integrated amplification grid and have a high efficiency to detect single ionisation electrons. In the test beam setup, the module was placed in between two sets of Mimosas26 silicon detector planes that provided external high precision tracking and the whole detector setup was slid into the PCMag magnet at DESY. The analysed data were taken at electron beam energies of 5 and 6 GeV and at magnetic fields of 0 and 1 Tesla(T).

The result for the transverse diffusion coefficient D_T is $287 \mu\text{m}/\sqrt{\text{cm}}$ at $B = 0$ T and D_T is $121 \mu\text{m}/\sqrt{\text{cm}}$ at $B = 1$ T. The longitudinal diffusion coefficient D_L is measured to be $268 \mu\text{m}/\sqrt{\text{cm}}$ at $B = 0$ T and $252 \mu\text{m}/\sqrt{\text{cm}}$ at $B = 1$ T. Results for the tracking systematical uncertainties in xy (pixel plane) were measured to be smaller than $13 \mu\text{m}$ with and without magnetic field. The tracking systematical uncertainties in z (drift direction) were smaller than $15 \mu\text{m}$ ($B = 0$ T) and $20 \mu\text{m}$ ($B = 1$ T). Finally, the result for the dE/dx resolution for a MIP particle based on a 1 meter track and a realistic GridPix coverage of 60% was measured to be 4% in a 1 T magnetic field.

Keywords: Micromegas, gaseous pixel detector, micro-pattern gaseous

*Corresponding author. Telephone: +31 20 592 2000
Email address: s01@nikhef.nl (P.M. Kluit)
Preprint submitted to Elsevier

30 **1. Introduction**

31 Earlier publications on a single chip [1] and four chip (quad) GridPix detec-
 32 tors [2] showed the potential of the GridPix technology and the large range of
 33 applications for these devices [3]. In particular, it was demonstrated that single
 34 ionisation electrons can be detected with high efficiency and great precision, al-
 35 lowing an excellent 3D track position measurements and particle identification
 36 based on the number of electrons and clusters.

37 As a next step towards a Pixel Time Projection Chamber for a future col-
 38 lider experiment [4], [5], a module consisting of 32 GridPix chips based on the
 39 Timepix3 chip was constructed.

40 A GridPix detector consists of a CMOS pixel Timepix3 chip [6] with inte-
 41 grated amplification grid added by Micro-electromechanical Systems (MEMS)
 42 postprocessing techniques. The Timepix3 chip can be operated with a low
 43 threshold of $515 e^-$, and has a low equivalent noise charge of about $70 e^-$.
 44 The GridPix single chip and quad detectors have a very fine granularity of
 45 $55 \mu\text{m} \times 55 \mu\text{m}$ and a high efficiency to detect single ionisation electrons.

46 Based on the experience gained with these detectors a 32 GridPix chip mod-
 47 ule - consisting of 8 quads - was built. A drift box defining the electric field
 48 and gas envelop was constructed. A readout system for up to 128 chips with 4
 49 multiplexers readout by one speedy pixel detector readout SPIDR board [7] [8]
 50 was designed. After a series of tests using the laser setup and cosmics in the
 51 laboratory at Nikhef [9], the detector was taken to DESY for a two week test
 52 beam campaign.

53 At DESY the 32 chip detector was placed in between two sets of Mimosa26
 54 silicon detector planes and mounted on a movable stage. The whole detector
 55 setup was slid into the centre of the PCMAG magnet at DESY. A beam
 56 trigger was provided by scintillator counters. The data reported here were taken
 57 at different stage positions and electron beam momenta of 5 and 6 GeV/c and

58 at magnetic fields of 0 and 1 T. The performance of the 32 GrixPix chip module
59 was measured using these data sets.

60 **2. 32 GridPix chip module**

61 A 32 GrixPix chip module was built using the quad module [2] as a basic
62 building block. The quad module consists of four GridPix chips and is optimised
63 for a high fraction of sensitive area of 68.9%. The external dimensions are
64 $39.60 \text{ mm} \times 28.38 \text{ mm}$. The four chips which are mounted on a cooled base plate
65 (COCA), are connected with wire bonds to a common central 6 mm wide PCB.
66 A 10 mm wide guard electrode is placed over the wire bonds 1.1 mm above the
67 aluminium grids, in order to prevent field distortions of the electric drift field.
68 The guard is the main inactive area, and its dimensions are set by the space
69 required for the wire bonds. On the back side of the quad module, the PCB
70 is connected to a low voltage regulator. The aluminium grids of the GridPixes
71 are connected by $80 \mu\text{m}$ insulated copper wires to a high voltage (HV) filtering
72 board. The quad module consumes about 8 W of power of which 2 W is used in
73 the LV regulator.

74 Eight quad modules were embedded in a box, resulting in a GridPix module
75 with a total of 32 chips. A schematic 3-dimensional drawing of the detector is
76 shown in Figure 1. A schematic drawing of the quads in the module is shown
77 in Figure 2, where also the beam direction is indicated.

78 The internal dimensions of the box are 79 mm along the x -axis, 192 mm along
79 the y -axis, and 53 mm along the z -axis (drift direction), and it has a maximum
80 drift length (distance between cathode and readout anode) of 40 mm. The drift
81 field is shaped by a series of parallel CuBe field wires of $75 \mu\text{m}$ diameter with a
82 wire pitch of 2 mm and guard strips are located on all of the four sides of the
83 active area. In addition, six guard wires - shown with dashed lines in Figure
84 2 - are suspended over the boundaries of the chips, where no guard is present,
85 to minimise distortions of the electric drift field. The wires are located at a
86 distance of 1.15 mm from the grid planes, and their potential is set to the drift

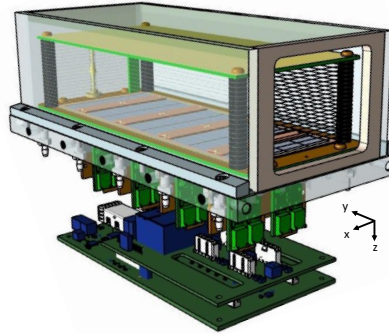


Figure 1: Schematic 3-dimensional render of the 8-quad module detector for illustration purposes.

87 potential at this drift distance. The box has two Kapton $50\ \mu\text{m}$ windows to
 88 allow the beam to pass with minimal multiple scattering.

89 The data acquisition system of the quad module was adopted to allow for
 90 multiple quads to be readout. A multiplexer card was developed that handles
 91 four quads or 16 chips and combines the Timepix3 data into one data stream.
 92 For the 32 GrixPix module two multiplexers are connected to a SPIDR board
 93 that controls the chips and readout process. The readout speed per chip is
 94 160 Mbps and for the multiplexer 2.56 Gbps this corresponds to a maximum

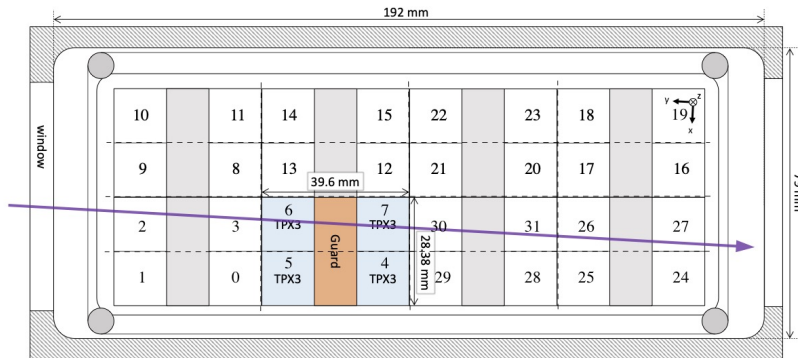


Figure 2: Schematic drawing of the 8-quad module detector with one example quad as viewed from the top of the quads. The chips are numbered and the beam direction is shown in purple.

95 rate of 21 MHits/s. For each pixel the precise Time of Arrival (ToA) using a
96 640 MHz TDC and the time over threshold (ToT) are measured.

97 The gas volume of 780 ml is continuously flushed at a rate of ~ 50 ml/min
98 (about 4 volumes/hour) with premixed T2K TPC gas. This gas is a mixture
99 consisting of 95 % Ar, 3 % CF_4 , and 2 % iC_4H_{10} suitable for large TPCs because
100 of the low diffusion in a magnetic field and the high drift velocity.

101 3. Experimental setup

102 In preparation of the two weeks DESY test beam campaign, a support frame
103 was designed to move the 32 chip GridPix module in the plane perpendicular to
104 the beam by a remotely controlled stage such that the whole detector volume
105 could be probed. The module was mounted upside down with respect to figure 1
106 thus that the electronics could be accessed from above. The support frame also
107 held three Mimosas26 silicon detector planes [10] - with an active area of (21.2
108 mm x 10.6 mm) - placed in front of the detector and three Mimosas26 planes
109 behind the detector. At DESY the (Mimosas26) silicon detector planes were
110 provided by the test beam coordinators. The whole detector setup was slid
111 towards the centre of the PCMAG magnet at the DESY test beam facility II
112 [10]. A beam trigger was provided by a double scintillator counter coincidence.
113 The data were taken at different stage positions to cover the whole sensitive
114 TPC volume. Runs with electron beam momenta of 5 and 6 GeV/c and at
115 magnetic fields of 0 and 1 T were analysed.

116 A photograph of the detector setup in the PCMAG magnet is shown in
117 Figure 3.

118 The experimental and environmental parameters such as temperature, pres-
119 sure, gas flow, oxygen content were measured and logged by a Windows op-
120 erated slow control system. The experimental parameters are summarised in
121 Table 1. The chips were cooled by circulating Glycol through the cooling chan-
122 nels in the module carrier plate. The cooling blocks of the multiplexers were
123 further cooled by blowing pressurised air on them.

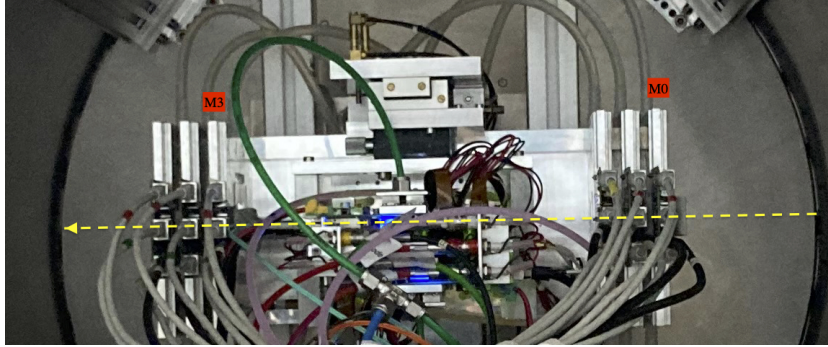


Figure 3: Photo of the detector setup at the centre of the PCMAG magnet. The Mimosa26 planes M0 and M3 are indicated in red as well as the beam direction (yellow). Centrally, the stager positions the TPC module to allow the beam to pass through.

Table 1: Overview of the experimental parameters. The ranges indicate the variation over the data taking period

Number of analysed runs at B=0 (1) T	6 (8)
Run duration	10-90 minutes
Number of triggers	3-100 k
E_{drift}	280 V/cm
V_{grid}	340 V
Threshold	550 e ⁻
Gas Temperature	303.3-306.6 K
Pressure	1011 – 1023 mbar
Oxygen concentration	240 - 620 ppm
Water vapour concentration	2000 - 7000 ppm

124 The data was produced in four main data streams: one stream produced by
125 the Mimosa26 Telescope, two data streams by the two Timepix multiplexers and
126 one trigger stream. The double scintillator coincidence provided a trigger signal
127 to the Trigger Logic Unit (TLU) [11] that sends a signal to the telescope readout
128 and the trigger SPIDR. The data acquisition system of the Telescope and trigger
129 SPIDR injected a time stamp into their respective data streams. Hits from the
130 Mimosa26 planes were collected with a sliding window of $-115\ \mu\text{s}$ to $230\ \mu\text{s}$ of
131 the trigger. The data acquisition of the multiplexer and the trigger SPIDR were
132 synchronised at the start of the run. By comparing the time stamps in these
133 streams, Telescope tracks and TPC tracks could be matched. Unfortunately,
134 the SPIDR trigger had - due to a cabling mistake at the output of the TLU - a
135 common 25 nsec time jitter.

136 In the first week of the test beam period it was found that three HV cables
137 had a bad connection. The cables were replaced and the module could be fully
138 operated. Unfortunately, after a short data taking period one of the chips (nr 11)
139 developed a short circuit and the HV on the grid of the chip was disconnected.
140 After the test beam data taking period the module was repaired in the clean
141 room in Bonn.

142 4. Analysis

143 4.1. Telescope Track reconstruction procedure

144 The data of the Telescope is decoded and analysed using the Corryvreckan
145 software package [12]. The track model used for fitting was the General Broken
146 Lines (GBL) software [13]. The code was extended and optimised to fit curved
147 broken lines for the data with magnetic field. The telescope planes were itera-
148 tively aligned using the standard alignment software provided by the package.
149 The single point Mimosa26 resolution is $4\ \mu\text{m}$ in x and $6\ \mu\text{m}$ in z (drift direction).

150 Telescope tracks were selected with at least 5 out of the 6 planes on the track
151 and a total χ^2 of better than 25 per degree of freedom. The uncertainties on the
152 Telescope track prediction in the middle of the GridPix module are dominated

153 by multiple scattering. The amount of multiple scattering was estimated by
 154 comparing the predictions from the two telescope arms for 6 GeV/c tracks at 0
 155 T. The expected uncertainty in x and z is 26 μm on average.

156 4.2. TPC Track reconstruction procedure

157 GridPx hits are selected requiring a minimum time over threshold ToT of
 158 0.15 μs . The drift time is defined as the measured time of arrival minus the
 159 trigger time recorded in the trigger SPIDR data stream minus a fixed t_0 (the
 160 drift time at zero drift). The drift time was corrected for time walk [2] using
 161 the measured time over threshold (ToT in units of μs) and the formula (1):

$$\delta t = \frac{18.6(ns)}{\text{ToT} + 0.1577}. \quad (1)$$

162 Furthermore, small time shift corrections - with an odd-even and a 16×2 pixels
 163 structure - coming from the TPX3 clock distribution were extracted from the
 164 data and applied.

165 The z drift coordinate was calculated as the product of the drift time and
 166 the drift velocity. This implies that $z_{\text{drift}} = -z$ as defined in figure 1. GridPix
 167 hits outside an acceptance window in x (± 15 mm) and z (± 7.5 mm) were
 168 not used in the track finding and reconstruction. Based on a Hough transform
 169 an estimate of the TPC track position and angles in the middle of the module
 170 (at $y = 1436$ pixels) was obtained. This estimate was used to collect the hits
 171 around the TPC track and fit the track parameters. For this fit a straight line
 172 (B=0 T) or a quadratic track (B=1 T) model was used. In the fit, the expected
 173 uncertainties per hit σ_x and σ_z were used. The fit was iterated three times to
 174 perform outlier removal at respectively 10, 5 and 2.5 sigma level. A TPC track
 175 was required to have a least 100 hits in each multiplexer. At least 25% of the
 176 total number of hits should be on track and the χ^2 per degree of freedom has
 177 to be less than 3 in xy and z. All track parameters were expressed at a plane
 178 the middle of the TPC.

179 The calibration and alignment of the detector was done using high quality
 180 tracks. The track selections are summarised in table 2.

Table 2: Table with track/event selection cuts

Track/Event Selection
$ x_{\text{TPC}} - x_{\text{Telescope}} < 0.3 \text{ mm}$
$ z_{\text{TPC}} - z_{\text{Telescope}} < 2.0 \text{ mm}$
$ dx/dy_{\text{TPC}} - dx/dy_{\text{Telescope}} < 4 \text{ mrad}$
$ dz/dy_{\text{TPC}} - dz/dy_{\text{Telescope}} < 2 \text{ mrad}$

181 The drift velocity was calibrated per run by fitting a linear function to the z
 182 (predicted from the Telescope track at the measured TPC hit position) versus
 183 the measured drift time in the TPC. For the B=0 field runs it varies between
 184 61.6 and 63.0 $\mu\text{m}/\text{ns}$. For the B=1 T runs it is between 57.2 and 59.1 $\mu\text{m}/\text{ns}$.
 185 The variation comes mainly from the changes in the relative humidity of the
 186 gas volume due to small leaks.

187 The individual TPX3 chips were iteratively aligned fitting a shift in x (z drift)
 188 and two slopes $dx(z \text{ drift})/d \text{ row}(\text{column})$. The alignment was done per run,
 189 because the detector was moved in x and/or z for each run. The fitted slopes
 190 also corrected for small shifts and rotations (3D) in the nominal chip position.

191 An example event run 6913 without B field with a TPC and a telescope
 192 track is shown in figure 4. The TPC is located between $y = 0$ and 2872 pixels.
 193 Three Mimosas26 planes are located at $y < -1000$ and three at $y > 4000$ pixels.

194 5. Hit resolutions

195 In order to study the single electron resolution for the data with and without
 196 magnetic field, additional selections on the Telescope and TPC tracks were
 197 applied. Due to the trigger time jitter of 25 nsec, the prediction of the telescope
 198 track in z must be used as the reference for z. Secondly, the z hits of the TPC
 199 track were fitted to correct for the common time shift and the z residuals were
 200 calculated with respect to the fitted TPC track. In the xy plane the residuals
 201 of TPC hits with respect to the telescope track were used to extract the single

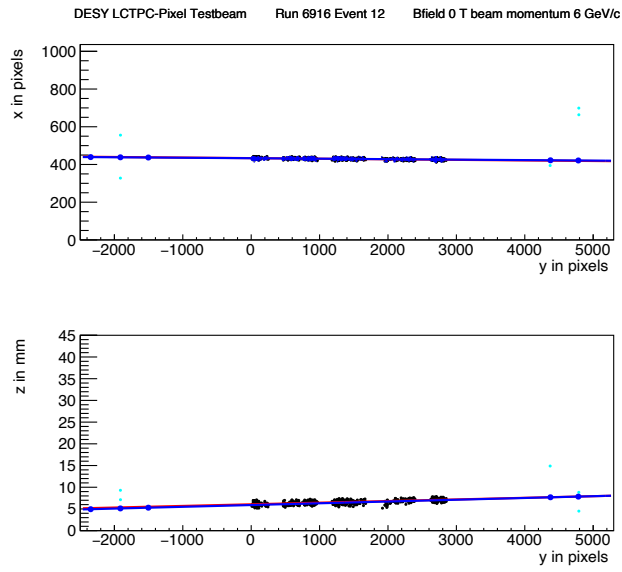


Figure 4: An event display for run 6913 without B field, with in total 1293 TPC hits (black dots) in the precision plane (xy) and driftplane (z drift y). The fitted TPC track (red line) with 1130 hits on track and the telescope track (blue line) with 5 Mimosa26 planes (blue hits) on track are shown. In green the off track Mimosa26 hits are shown.

202 electron resolution in xy . For the resolution studies runs at three different z stage
 203 positions of the TPC were selected where the beam gave hits in the central chips.
 204 The data of 14 central chips (9, 12, 21, 20, 17, 16, 2, 3, 6, 7, 30, 31, 26 and 27)
 205 was used. Two chips (8 and 13) were left out because of the E field deformations
 206 caused by the short circuit in chip 11.

207 5.1. Hit resolutions in the pixel plane

208 The resolution of the hits in the pixel plane (xy) was measured as a function
 209 of the predicted drift position (z_{drift}). Only hits are used crossing the fiducial
 210 region defined by the central core of the beam and staying 20 pixels away from
 211 the chip edges. The resolution for the detection of ionisation electrons σ_x is
 212 given by:

$$\sigma_x^2 = \frac{d_{\text{pixel}}^2}{12} + d_{\text{track}}^2 + D_T^2(z_{\text{drift}} - z_0), \quad (2)$$

213 where d_{pixel} is the pixel pitch size, d_{track} the uncertainty from the track predic-
 214 tion, z_0 is the position of the grid, and D_T is the transverse diffusion coefficient.
 215 The resolution at zero drift distance $d_{\text{pixel}}/\sqrt{12}$ was fixed to 15.9 μm and d_{track}
 216 to 30 μm for B=0 and 42 μm for B = 1 T data.

217 The expression (2) - leaving z_0 and the D_T as free parameters - is fitted to
 218 the B=0 T data shown in Figure 5. The fit gives a transverse diffusion coefficient
 219 D_T of 287 $\mu\text{m}/\sqrt{cm}$ with negligible statistical uncertainty. The measured value
 220 is in agreement with value of 287 $\mu\text{m}/\sqrt{cm} \pm 4\%$ predicted by the gas simulation
 221 software Magboltz [15]. The values of the diffusion coefficients depend on the
 222 humidity that was not precisely measured during the testbeam. The humidity
 223 strongly affects the drift velocity. Therefore the drift velocity prediction from
 224 Magboltz was used to determine the water content per run and predictions for
 225 the diffusion coefficients could be obtained.

226 A fit to the B=1 T data shown in Figure 5 gives a transverse diffusion
 227 coefficient D_T of 121 $\mu\text{m}/\sqrt{cm}$ with negligible statistical uncertainty. The mea-
 228 sured value is in agreement with the value of 119 $\mu\text{m}/\sqrt{cm} \pm 2\%$ predicted by
 229 Magboltz.

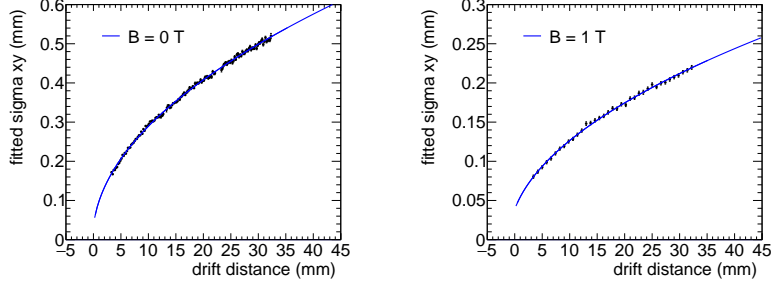


Figure 5: Measured hit resolution in the pixel plane (black points) fitted with the resolution function according to equation (2) (blue line).

230 *5.2. Hit resolution in the drift plane*

231 The resolution for the detection of ionisation electrons σ_z in the drift plane
 232 is given by:

$$\sigma_z^2 = \sigma_{z0}^2 + d_{\text{track}}^2 + D_L^2(z_{\text{drift}} - z_0), \quad (3)$$

233 where σ_{z0} is the resolution at zero drift distance, d_{track} the expected track
 234 uncertainty and D_L the longitudinal diffusion constant. Only track crossing
 235 the fiducial region were accepted and hits with a ToT value above $0.6 \mu\text{s}$ were
 236 selected. Because of the time jitter, the fitted TPC track is used for the drift
 237 residuals. For z_{drift} the Telescope prediction at the hit was used. The expected
 238 uncertainty on the Telescope track prediction is $25 \mu\text{m}$ at $z = 0 \text{ mm}$ and $75 \mu\text{m}$
 239 at $z = 30 \text{ mm}$.

240 The expression (3) - leaving σ_{z0} and the D_L as free parameters - is fitted
 241 to the B=0 T data shown in Figure 6. The value of z_0 was fixed to the result
 242 of the fit in the xy plane. The value of σ_{z0} was measured to be $138 \mu\text{m}$. The
 243 longitudinal diffusion coefficient D_L was determined to be $265 \pm 1 \mu\text{m}/\sqrt{\text{cm}}$,
 244 which is higher than the expected value $236 \pm 3 \mu\text{m}/\sqrt{\text{cm}}$ from a Magboltz
 245 calculation [15].

246 A fit to the B=1 T data shown in Figure 6 gives a longitudinal diffusion
 247 coefficient D_L of $250 \pm 2 \mu\text{m}/\sqrt{\text{cm}}$. The measured value is in agreement with
 248 the value of $245 \pm 4 \mu\text{m}/\sqrt{\text{cm}}$ predicted by Magboltz. The fitted value of σ_{z0}

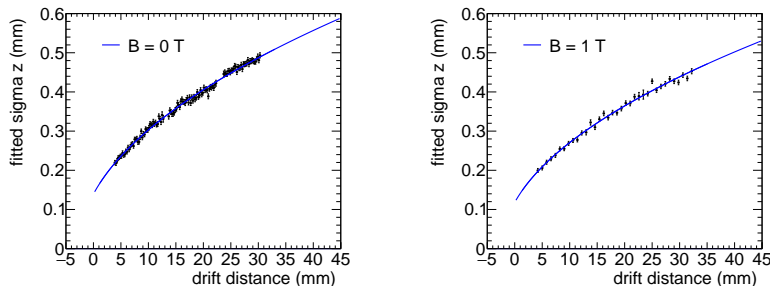


Figure 6: Resolution in the drift plane for hits with a ToT above $0.60 \mu\text{s}$. The data are fitted with the expression of equation (3).

249 was $133 \mu\text{m}$.

250 5.3. Deformations in the pixel and drift plane

251 It is important to measure possible deformations in the pixel (xy) and drift
 252 (z) plane to quantify the tracking precision. For the construction of a large
 253 Pixel TPC, deformations in the pixel plane deformation should be controlled to
 254 better than typically $20 \mu\text{m}$ because these affect the momentum resolution. The
 255 mean residuals in the pixel and drift planes are shown in figure 7 for the $B=0 \text{ T}$
 256 data set using a large set of runs to cover the whole module. The residuals were
 257 calculated with respect to the Telescope track prediction. Because of limited
 258 statistics bins were grouped into 8×16 pixels. Bins with less than 100 hits are
 259 left out and residuals larger (smaller) than $(-)100 \mu\text{m}$ are shown in red (blue).

260 A few critical areas can be observed in figure 7: the region around chip 11
 261 is affected (chips 14,8 and 13), because the grid of chip 11 was disconnected.
 262 Deformations are present at the four corners of the drift box (chips 24, 10, 1 and
 263 19) and close to the upper corner edge (chip 16) of the drift box. These come
 264 from inhomogenities in the drift field near the supporting pillars, the field wires
 265 are too close to the chip to provide a constant electric field. It was concluded
 266 that for the deformation results the hits of these nine chips have to be removed.
 267 The track fit was redone leaving these hits out of the fit, thus that they
 268 could not bias and affect the results.

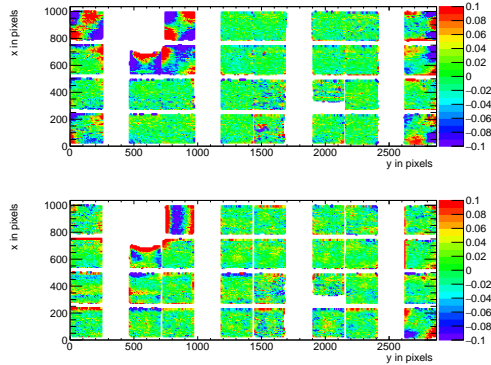


Figure 7: Mean residuals in the pixel and drift plane for $B=0$ T data at the expected hit position.

269 In order to reduce the statistical fluctuations and quantify the tracking pre-
 270 cision, the module was regrouped horizontally in four (mcol runs from 0 till 3
 271 along the local x axis) 256×256 pixel planes as shown in figure 8. Bins have a
 272 size of 16×16 pixels and bins with less than entries 1000 are not shown. A bias in
 273 the mean residual at the edge of the chips is expected to be present for an ideal
 274 detector because of the finite coverage and the diffusion in the drift process.
 275 Due to the presence of the dike pixels at the edge of the chip became covered
 276 and inefficient. Therefore the region near the edge of 5 pixels was removed. For
 277 the drift coordinate a region of 10 pixels was removed. The total number of
 278 measurements (bins) in xy is 895 and in z 892. One can observe that in the
 279 module plane no clear systematic deviations are present and conclude that the
 280 guard wire voltages were on average well tuned. Note that in the quad module
 281 we had no guard wires and deformation corrections had to be applied [2]. The
 282 r.m.s. of the distribution of the measured mean residual over the surface in
 283 the pixel plane is $11 \mu\text{m}$ and in the drift plane $15 \mu\text{m}$. Similarly, regrouping the
 284 module in four vertical planes of 256×256 pixels yielded a r.m.s. in the pixel
 285 plane of $13 \mu\text{m}$ and $13 \mu\text{m}$ in the drift coordinate. The expected statistical error
 286 in xy is $4 \mu\text{m}$ and in z $5 \mu\text{m}$.

287 In the $B=1$ T data set, the electrons will drift mainly along the magnetic

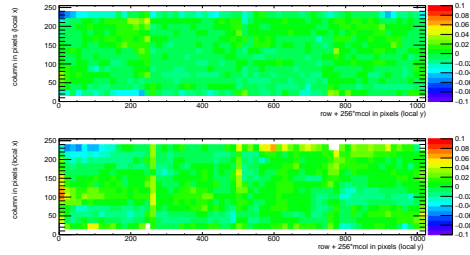


Figure 8: Mean residuals in the pixel and drift plane for B=0 T data at the regrouped expected hit position.

288 field lines. Deformations are in that case due to e.g. the non-alignment of the
 289 electric and magnetic field, giving ExB effects. Unfortunately, the statistics of
 290 the Telescope tracks that have a matched TPC track was insufficient and did
 291 not cover the full TPC module plane. Therefore the larger statistics of matched
 292 and unmatched TPC tracks was used. TPC tracks were required to pass angular
 293 selection cuts (dx/dy between -40 and -20 mrad and dz/dy between 0 and 14
 294 mrad) and a momentum cut ($p > 2$ GeV and $q < 0$).

295 The mean residuals in the pixel and drift planes are shown in figure 9 for
 296 the B=1 T data set using a large set of runs to cover the whole module. The
 297 residuals were calculated with respect to the TPC track prediction. Because of
 298 limited statistics bins were grouped into 8×16 pixels. Bins with less than 100
 299 hits are left out and residuals larger (smaller) than (-)100 μm are shown in red
 300 (blue).

301 In figure 9 the critical areas discussed above - around chip 11, the four corner
 302 chips and chip 16 in the upper corner edge - can be clearly observed. For the
 303 deformation results the hits of these nine chips have to be removed. The TPC
 304 track fit was redone leaving these hits out of the fit, thus that they could
 305 not bias and affect the results. The TPC plane is well covered, although one
 306 can observe that due to the angle of the beam in the xy plane the chips in the
 307 upper right and lower left corners are not fully covered.

308 In order to reduce the statistical fluctuations and quantify the tracking pre-
 309 cision, the module was regrouped horizontally in four (mcid runs from 0 till 3

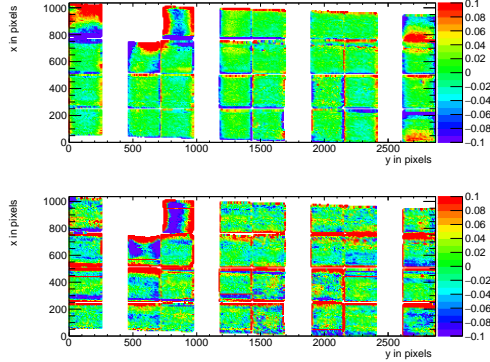


Figure 9: Mean residuals in the pixel and drift plane for B=1 T data at the expected hit position.

310 along the local x axis) 256x256 pixel planes as shown in figure 10. Bins have a
 311 size of 16x16 pixels and bins with less than entries 1000 are not shown. Similar
 312 to the nofield deformations studies, acceptance cuts had to be applied. The
 313 region near the edge of 16 pixels (columns) was removed. For the drift coordi-
 314 nate in addition a region of 10 pixels (rows) was removed. The total number
 315 of measurements (bins) in xy is 896 and in z 896. One can observe that in
 316 the module plane no clear systematic deviations are present. The r.m.s. of the
 317 distribution of the measured mean residual over the surface in the pixel plane
 318 is 13 μm and in the drift plane 19 μm . Similarly, regrouping the module in four
 319 vertical planes of 256x256 pixels yielded a r.m.s. in the pixel plane of 11 μm and
 320 20 μm in the drift coordinate. The expected statistical error in xy is 2 μm and
 321 in z 3 μm .

322 5.4. Tracking resolution

323 A selected TPC track in the B=0 T data has on average 1000 hits. The
 324 tracking precision in the middle of the TPC was derived on a track by track
 325 and found to be on average 9 μm in the precision plane and 13 μm in z. The
 326 angular resolution in dx/dy was on average 0.19 mrad and for dz/dy 0.25 mrad.
 327 It is clear that the position resolution in the TPC in the precision and drift
 328 coordinates is impressive for a tracklength of (only) 158 mm. The values are

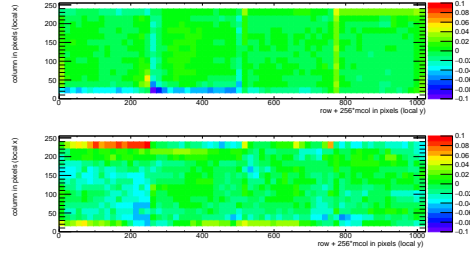


Figure 10: Mean residuals in the pixel and drift plane for B= 1T data at the regrouped expected hit position.

329 smaller than the uncertainty on the track prediction from the silicon telescope
 330 of 26 μm on average that is dominated by multiple scattering.

331 6. Particle Identification using dE/dx

332 The distribution of the number of TPC track hits per chip - without requiring
 333 a matched Telescope track - are shown in figure 11 for the data without magnetic
 334 field and for the B = 1 T data. The B=0 T data selects chips 2,6,7,9,16,17,26
 335 and 27. The B=1 T data selects the same chips plus chips 12,13,20 and 21.

336 The mean number of hits is measured to be 124 and 89 in the B=0 and
 337 1 T data sets. The most probable values are respectively 87 and 64. Note
 338 that the B=0 data has a much larger Landau-like tail than the 1 T data. Also
 339 the fluctuations in the core of the distribution are larger. The mean time over
 340 threshold for the B=0 T is 0.68 μs and 0.86 μs at a 1 T field. This means that the
 341 deposited charge per pixel is smaller for the 0 T data. The most probable value
 342 for the total deposited charge is similar for both data sets. The mean number
 343 of hits is in agreement with the predictions of [14] 106 electron-ion pairs for a
 344 6 GeV/c electron at B=0 T , crossing 236 pixels or 12.98 mm and a detector
 345 running at 85% single electron efficiency.

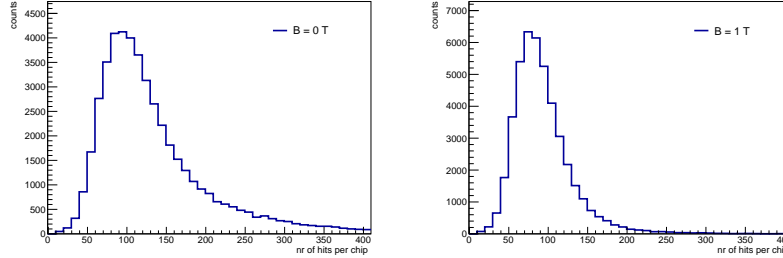


Figure 11: Distribution of the number of track hits per per chip for B=0 (left) B=1 T data.

346 7. Conclusion and outlook

347 A Time Projection Chamber module with 32 GridPix chips was constructed
 348 and the performance was measured using data taken in a test beam at DESY
 349 in 2021. The analysed data were taken at electron beam momenta of 5 and 6
 350 GeV/c and at magnetic fields of 0 and 1 T.

351 The result for the transverse diffusion coefficient D_T is $287 \mu\text{m}/\sqrt{\text{cm}}$ at B =
 352 0 T and D_T is $121 \mu\text{m}/\sqrt{\text{cm}}$ at B = 1 T. The longitudinal diffusion coefficient
 353 D_L is measured to be $268 \mu\text{m}/\sqrt{\text{cm}}$ at B = 0 T and $252 \mu\text{m}/\sqrt{\text{cm}}$ at B = 1 T.
 354 Results for the tracking systematical uncertainties in xy were measured to be
 355 smaller than $13 \mu\text{m}$ with and without magnetic field. The tracking systematical
 356 uncertainties in z were smaller than $15 \mu\text{m}$ (B = 0 T) and $20 \mu\text{m}$ (B = 1 T).

357 Acknowledgements

358 The 32 Gridpix module could not be constructed without the enormous effort
 359 and creative energy that Fred Hartjes has invested in it over several years. This
 360 research was funded by the Netherlands Organisation for Scientific Research
 361 NWO. The authors want to thank the support of the mechanical and electronics
 362 departments at Nikhef and the detector laboratory in Bonn. The measurements
 363 leading to these results have been performed at the Test Beam Facility at DESY
 364 Hamburg (Germany), a member of the Helmholtz Association (HGF).

365 **References**

- 366 [1] C. Ligtenberg, et al., Performance of a GridPix detector based on the
367 Timepix3 chip, Nucl. Instrum. Meth. A 908 (2018) 18–23. [arXiv:1808.04565](#),
368 [doi:10.1016/j.nima.2018.08.012](#).
- 369 [2] C. Ligtenberg, et al., Performance of the GridPix detector quad, Nucl.
370 Instrum. Meth. A 956 (2020) 163331. [arXiv:2001.01540](#), [doi:10.1016/j.nima.2019.163331](#).
371
- 372 [3] J. Kaminski, Y. Bilevych, K. Desch, C. Krieger, M. Lupberger, GridPix de-
373 tectors - introduction and applications, Nucl. Instrum. Meth. A845 (2017)
374 233–235. [doi:10.1016/j.nima.2016.05.134](#).
- 375 [4] C. Ligtenberg, A GridPix TPC readout for the ILD experiment at the
376 future International Linear Collider, Ph.D. thesis, Free University of
377 Amsterdam (2021).
378 URL [https://www.nikhef.nl/pub/services/biblio/theses_pdf/](https://www.nikhef.nl/pub/services/biblio/theses_pdf/thesis_C_Ligtenberg.pdf)
379 [thesis_C_Ligtenberg.pdf](https://www.nikhef.nl/pub/services/biblio/theses_pdf/thesis_C_Ligtenberg.pdf)
- 380 [5] M. Lupberger, Y. Bilevych, H. Blank, D. Danilov, K. Desch, A. Hamann,
381 J. Kaminski, W. Ockenfels, J. Tomtschak, S. Zigann-Wack, Toward the
382 Pixel-TPC: Construction and Operation of a Large Area GridPix Detector,
383 IEEE Trans. Nucl. Sci. 64 (5) (2017) 1159–1167. [doi:10.1109/TNS.2017.2689244](#).
384
- 385 [6] T. Poikela, J. Plosila, T. Westerlund, M. Campbell, M. De Gaspari,
386 X. Llopart, V. Gromov, R. Kluit, M. van Beuzekom, F. Zappone,
387 V. Zivkovic, C. Brezina, K. Desch, Y. Fu, A. Kruth, Timepix3: a 65K
388 channel hybrid pixel readout chip with simultaneous ToA/ToT and sparse
389 readout, JINST 9 (05) (2014) C05013.
390 URL <http://stacks.iop.org/1748-0221/9/i=05/a=C05013>
- 391 [7] J. Visser, M. van Beuzekom, H. Boterenbrood, B. van der Heijden, J. I.
392 Muñoz, S. Kulis, B. Munneke, F. Schreuder, SPIDR: a read-out system for

- 393 Medipix3 & Timepix3, Journal of Instrumentation 10 (12) (2015) C12028.
394 doi:10.1088/1748-0221/10/12/C12028.
- 395 [8] B. van der Heijden, J. Visser, M. van Beuzekom, H. Boterenbrood, S. Kulis,
396 B. Munneke, F. Schreuder, SPIDR, a general-purpose readout system for
397 pixel ASICs, JINST 12 (02) (2017) C02040. doi:10.1088/1748-0221/12/
398 02/C02040.
- 399 [9] F. Hartjes, A diffraction limited nitrogen laser for detector calibration in
400 high energy physics, Ph.D. thesis, University of Amsterdam (1990).
401 URL [https://www.nikhef.nl/pub/services/biblio/theses_pdf/
402 thesis_F_Hartjes.pdf](https://www.nikhef.nl/pub/services/biblio/theses_pdf/thesis_F_Hartjes.pdf)
- 403 [10] R. Diener et al., The DESY II test beam facility, Nuclear Instruments
404 and Methods in Physics Research. Section A: Accelerators, Spectrometers,
405 Detectors and Associated Equipment 922 (2019) 265–286. arXiv:1807.
406 09328, doi:10.1016/j.nima.2018.11.133.
- 407 [11] P. Baesso, D. Cussans, J. Goldstein, The AIDA-2020 TLU: a flexible trigger
408 logic unit for test beam facilities, Journal of Instrumentation 14 (09) (2019)
409 P09019–P09019. doi:10.1088/1748-0221/14/09/p09019.
410 URL <https://doi.org/10.1088/1748-0221/14/09/p09019>
- 411 [12] D. Dannheim, K. Dort, L. Huth, D. Hynds, I. Kremastiotis, J. Kröger,
412 M. Munker, F. Pitters, P. Schütze, S. Spannagel, T. Vanat, M. Williams,
413 Corryvreckan: a modular 4d track reconstruction and analysis software
414 for test beam data, Journal of Instrumentation 16 (03) (2021) P03008.
415 doi:10.1088/1748-0221/16/03/p03008.
416 URL <https://doi.org/10.1088/1748-0221/16/03/p03008>
- 417 [13] C. Kleinwort, General broken lines as advanced track fitting method, Nu-
418 clear Instruments and Methods in Physics Research Section A: Accelerators,
419 Spectrometers, Detectors and Associated Equipment 673 (2012) 107–
420 110. doi:10.1016/j.nima.2012.01.024.

- 421 [14] R. Veenhof, Garfield - simulation of gaseous detectors, version 9, Reference
422 W5050 (1984-2010).
423 URL <https://garfield.web.cern.ch>
- 424 [15] S. F. Biagi, Monte Carlo simulation of electron drift and diffusion in count-
425 ing gases under the influence of electric and magnetic fields, Nucl. Instrum.
426 Meth. A421 (1-2) (1999) 234–240. doi:10.1016/S0168-9002(98)01233-9.
427 URL <https://magboltz.web.cern.ch/magboltz>